Catálisis, cinética y reactores

Revista Mexicana de Ingeniería Química
Vol. 13, No. 2 (2014) 473-481

ELECTRON PARAMAGNETIC RESONANCE (EPR) INVESTIGATION OF TiO_2-DELAMINATED CLAYS

INVESTIGACIÓN POR RESONANCIA PARAMAGNÉTICA ELECTRÓNICA (EPR) DE ARCILLAS DELAMINADAS CON TiO_2

J.G. Carriazo[1]*, A. Ensuncho-Muñoz[2] and O. Almanza[3]

[1]*Departamento de Química, Universidad Nacional de Colombia, Sede Bogotá. Ciudad Universitaria, Carrera 30, Nº 45-03, Bogotá, D. C. (Colombia).*
[2]*Departamento de Química, Facultad de Ciencias Básicas e Ingeniería, Universidad de Córdoba. Montería, Colombia.*
[3]*Departamento de Física, Universidad Nacional de Colombia, Sede Bogotá. Ciudad Universitaria, Carrera 30, Nº 45-03, Bogotá, D. C. (Colombia).*

Received February 16, 2013; Accepted March 15, 2014

Abstract

In this paper a set of TiO_2 and Fe/TiO_2 delaminated clays, prepared by different synthesis procedures, was characterized by electron paramagnetic resonance (EPR) spectroscopy. EPR analyses revealed an important shift of the central g-value as consequence of Fe^{3+} insertion (substitution) in the TiO_2 structure by a sensitive and direct method of iron incorporation. A series of additional g-values, symmetrically distributed around the central absorption line, was attributed to some electron trapping sites (defects) remained in the TiO_2 framework. The spectroscopic characterizations carried out in this work contribute to understand the photo-catalytic properties previously observed for these solids.

Keywords: delaminated clay, titanium dioxide, EPR, iron-titanium modified clay, clay mineral.

Resumen

El presente artículo muestra la caracterización, mediante espectroscopía de resonancia paramagnética electrónica (EPR), de un conjunto de arcillas delaminadas con TiO_2 y Fe/TiO_2 obtenidas por diferentes procedimientos de síntesis. Los análisis de EPR mostraron un desplazamiento importante del valor "g" central como consecuencia de la inserción de Fe^{3+} por substitución en la estructura de TiO_2 mediante un método sensible y directo de incorporación de los iones hierro (III). Adicionalmente, se observó un conjunto de valores g simétricamente distribuidos alrededor de la línea del valor g central, las cuales se atribuyen a sitios de electrones atrapados en vacancias (defectos) de la estructura de TiO_2. La caracterización espectroscópica realizada en este trabajo contribuye a la comprensión de las propiedades fotocatalíticas previamente observadas para los sólidos sintetizados.

Palabras clave: arcilla delaminada, dióxido de titanio, EPR, arcilla modificada con hierro-titanio, mineral de arcilla.

1 Introduction

Nowadays, several technological procedures have been developed in the entire world in order to eliminate some toxic organic compounds (phenol, substituted phenols carboxylic acids, pesticides and herbicides, among others) which are poured into residual waters from chemical, agrochemical, petrochemical or pharmaceutical industries (Perathoner and Centi, 2005; Bhargava *et al*., 2006; Liotta *et al*., 2009). Adsorption processes, biological methods and those based on catalytic oxidation (homogeneous and heterogeneous) are worthy of mention, but in the heterogeneous-catalysis procedures those photo-assisted by ultraviolet-light (UV) are currently important (Carriazo *et al*., 2005; Carriazo *et al*., 2008; Yang *et al*., 2008; Iurascu *et al*., 2009).

*Autor para la correspondencia. *E-mail*: jcarriazog@unal.edu.co

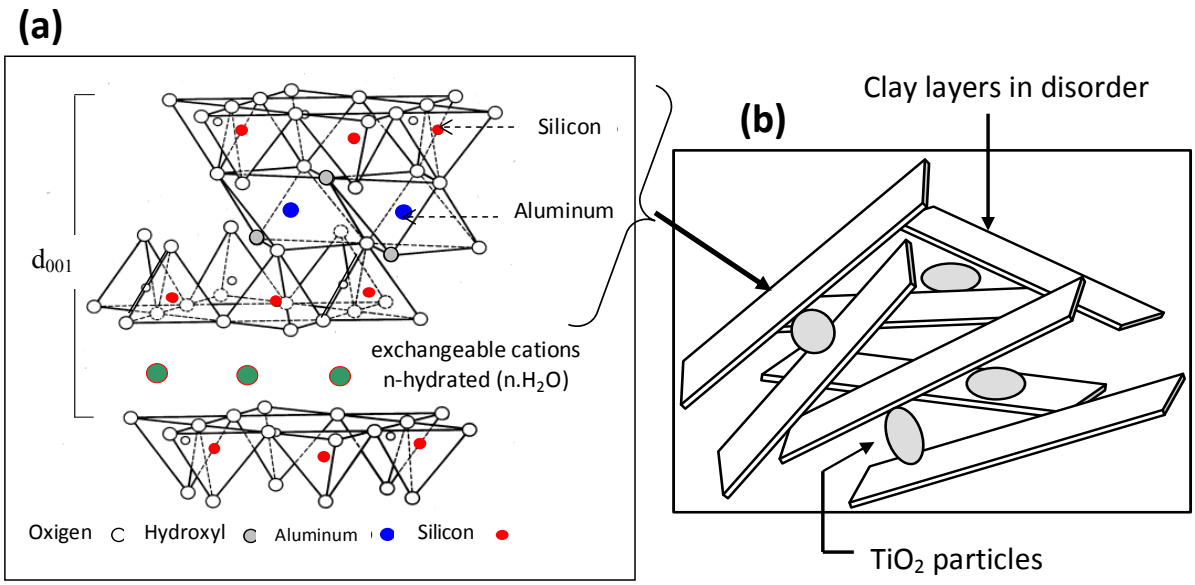

Fig. 1. Schematic representation of a smectite-type clay mineral (a), and a model of the delaminated-clay microstructure obtained by intercalation of TiO_2 (b).

Recently, photo-catalysts based on TiO_2 and Fe-TiO_2-delaminated clays were designed and a set of inorganic structure materials with higher or minor activity, depending on the synthesis procedure used to incorporate the iron species, were obtained (Carriazo *et al*., 2010). Such materials allow 1) optimizing the TiO_2 semiconductor (anatasa) by means of its dispersion on an appropriate and inexpensive solid matrix (clay mineral), and 2) shifting the band-gap value toward the visible spectrum through structural incorporation of Fe^{3+} ions (Crittenden *et al*., 1997; Pal *et al*., 1999; Liu *et al*., 2005; Ambrus *et al*., 2008; Ye *et al*., 2008). The last criterion allows advancing to a possible technological application of these catalytic systems, to be used under solar light irradiation. Figure 1 shows both the structure of a clay mineral (smectite) used in the preparation of these materials and a representative model of the delaminated clay structure obtained.

Regarding the effect of iron incorporation in TiO_2 (anatase) to enhance its photo-catalytic activity, the scientific literature has shown opposite results which have generated an enormous controversy on this subject (Di Paola *et al*., 2002; Zhu *et al*., 2004; Zhu *et al*., 2006; Ambrus *et al*., 2008; Liu and Chen, 2009), but in a previous work it was demonstrated that the sensitivity of this kind of solid structures to the UV absorption in a catalytic process is strongly dependent on the preparation method (Carriazo *et al*., 2010).

From a structural point of view, we consider that the incorporation of a metal ion (Fe^{3+}) inside the anatase framework is required as an essential condition to reach a modification of the band-gap value in order to shift it toward values close to the visible light region, for obtaining favorable effects on the photo-catalytic activity of modified TiO_2. Since this perspective, the progress on the study of our designed structures, by spectroscopic techniques sensitive to the metal ion (and its concentration level) introduced in the solids, is needed. For that reason, the present work explores the structural environments of iron species by using the electron paramagnetic resonance (EPR) spectroscopy.

EPR is a spectroscopic technique frequently used to investigate the structure and interactions of paramagnetic species (molecules or ions with unpaired electrons) such as free radicals, some metal ions and solid defects like electrons trapped in lattice vacancies. Therefore, EPR has been widely applied in the study of structural modification of titanium dioxide (both anatase and rutile): metal ion substitutions (for instance Fe^{3+}, Cu^{2+}, Mn^{4+}, etc.) and the elucidation of several kinds of structural defects (Cordischi *et al*., 2000; Janes *et al*., 2004; Hurum *et al*., 2006; Soria *et al*., 2007; Chong *et al*., 2008; Güler *et al*., 2009; Wang *et al*., 2011).

Finally, a solid structure deep knowledge of the studied catalysts will allow obtaining higher

information needed to optimize and develop possible technological applications of those catalytic systems. In this way, the aim of this work is to explore by EPR spectroscopy the structure of TiO_2 and Fe/TiO_2 nanoparticles included in the as-prepared delaminated clays.

2 Material and methods

2.1 Synthesis of solids

The detailed procedure of synthesis has already been published elsewhere (Carriazo *et al*., 2010). The catalysts were prepared by modification of the clay mineral (bentonite) previously characterized. Bentonite is a type of clay whose major component (a very high content) is the smectite clay mineral, thus the term "bentonite" indicates that the mineral modified in this work was smectite. Particles of 2 μm or less were selected and then "homoionized" with 1 M NaCl solution. The preparation of a Ti(IV) intercalating solution was carried out: 60 mL of $TiCl_4$ (60 wt.% in HCl) were slowly added to a beaker containing 70 mL of 37% HCl, with subsequent addition of distilled water (drop-wise and continuous stirring) to obtain a 0.85 M Ti solution.

2.1.1. Modification of the clay mineral via intercalation with Ti(IV) species: Ti?PILC solid

Sodium bentonite (20 g) was dispersed in 1 L of distilled water and the mixture was stirred for 24 h. The Ti(IV)-intercalating solution was slowly added to the bentonite suspension with vigorous stirring, up to a ratio of 10 mmol of Ti per gram of clay. The contact time of clay with the intercalating solution was 18 h. The Ti-modified clay was separated from solution by centrifugation and then washed several times with distilled water until the conductivity of the supernatant solution was close to that of distilled water. The final sample was dried at 60 °C and then calcined at 400 °C for 2 h in air static atmosphere.

2.1.2. Modification of the clay mineral via intercalation with Fe(III)-Ti(IV) species: Fe-Ti-PILC solid

An aqueous Ti-Fe solution was prepared to modify the clay mineral: 59 mL of Ti(IV)-intercalating solution were mixed with 100 mL of $Fe(NO_3)_3$ 0.5 M solution. The new Fe-Ti-intercalating solution was slowly added to a volume of the bentonite suspension maintaining a ratio of 10 mmol Ti/g of clay. The final sample was dried at 60 °C and then calcined at 400 °C for 2 h in air static atmosphere.

2.1.3 Incorporation of Fe(III) by cationic exchange: Fe-Ti-CE solid

This solid was synthesized using a typical cationic exchange procedure: 5 g of the solid Ti?PILC were dispersed in 250 mL of distilled water for 24 h with continuous stirring. Iron(III) nitrate (53 mmol of Fe^{3+}/g solid) was added to this suspension. The final solid was washed until the conductivity of the solution was close to that of distilled water, dried at 60 °C and then calcined at 400 °C for 2 h.

2.1.4. Incorporation of Fe(III) by impregnation: Fe-Ti-IMP solid

This solid was prepared by wet impregnation of Fe^{3+} ions on the solid Ti-PILC: 5.3 mmol of Fe^{3+} (as $Fe(NO_3)_3$) per gram of clay were added to a dilute Ti-PILC suspension in water under continuous stirring. The mixture was stirred for 3 h and then dried at 60 °C to be calcined at 400 °C for 2 h to obtain the final solid.

2.2 Characterization technique

EPR analyses were performed at room temperature in a Bruker ESP 300 spectrometer. EPR measurements were conducted with a modulation frequency of 100 kHz, a sweep width of 100 G, modulation amplitude of 0.49 G, scan time of 41.94 s, and microwave power of 20 mW. The calibration of this equipment was verified by radical cation $ABTS^{\bullet+}$ solutions: the initial concentration was prepared by dissolving 38.4 mg of ABTS (7.0 mM) and 6.6 mg of potassium persulfate (2.45 mM) in 10 mL of demineralized water (Re *et al*., 1999), and the additional concentrations were obtained by dilution. The characteristic g value for ABTS, measured under the given experimental conditions, was 2.008 (on a field of 3479 gauss) (Figure 2). This g value was in agreement with that reported in the literature (Scott *et al*., 1993; Zalibera *et al*., 2008), confirming the good operation level of the EPR spectrometer. For analyzing all the samples a frequency of 9.44 GHz was used, and the g-values were obtained from $g=h\nu/\beta H$, where β is the Bohr magneton, h is the Planck constant, ν is the frequency, and H is the center field at which the resonance occurs.

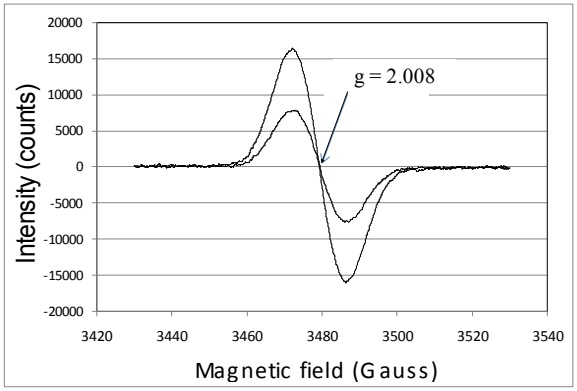

Fig. 2. EPR spectra of ABTS$^{\bullet+}$ radical for two concentrations.

3 Results and discussion

The synthesized materials were characterized by X-ray powder diffraction, X-ray fluorescence and IR spectroscopy in previous work (Carriazo *et al*., 2010), confirming their delaminated structure and the incorporation of titanium and iron-titanium oxides. In that work, the more active photocatalytic materials were Ti-PILC and Fe-Ti-PILC, this later showing a higher performance. On the other hand, metals such as Mn and Cr were not detected in the clay mineral (Carriazo *et al*., 2007).

Figure 3 shows the EPR spectra of the natural bentonite and the synthesized solids. In all cases the characteristic g values corresponding to iron species contained in the clay mineral (natural bentonite) were observed (Carriazo *et al*., 2008). The value of g=4.270 has been assigned in the literature to Fe^{3+} species isolated in either tetrahedral or octahedral symmetry with rhombic distortion (Kucherov and

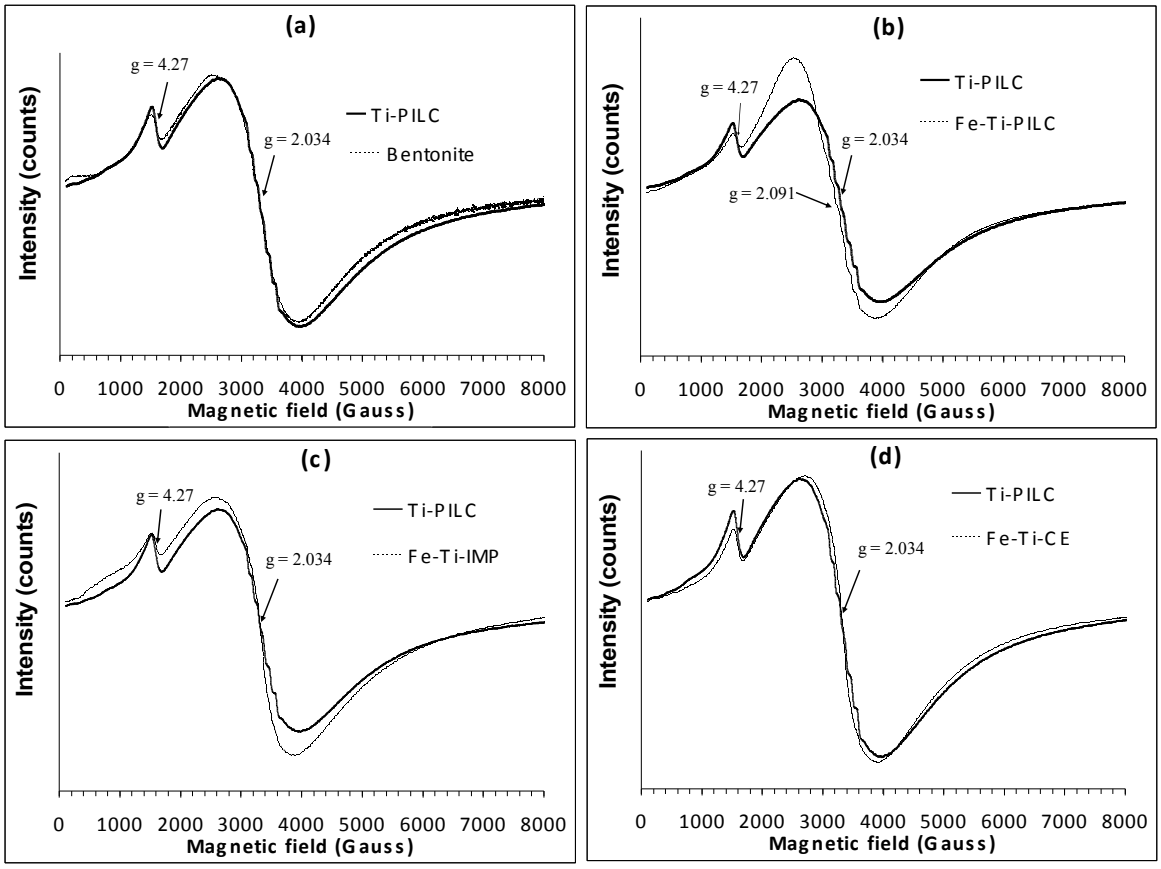

Fig. 3. EPR spectra of natural bentonite and delaminated clays synthesized by incorporation of Ti or Ti-Fe species using different procedures.

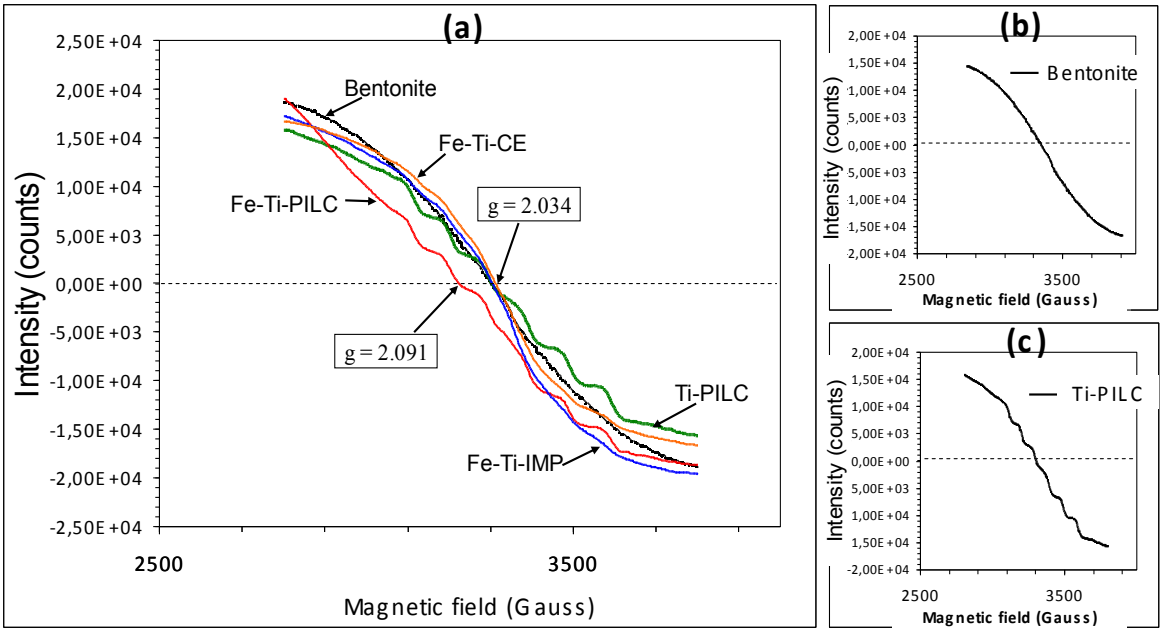

Fig. 4. EPR-spectra central lines (central g-values) of natural bentonite and delaminated clays synthesized by incorporation of Ti or Ti-Fe species using different procedures.

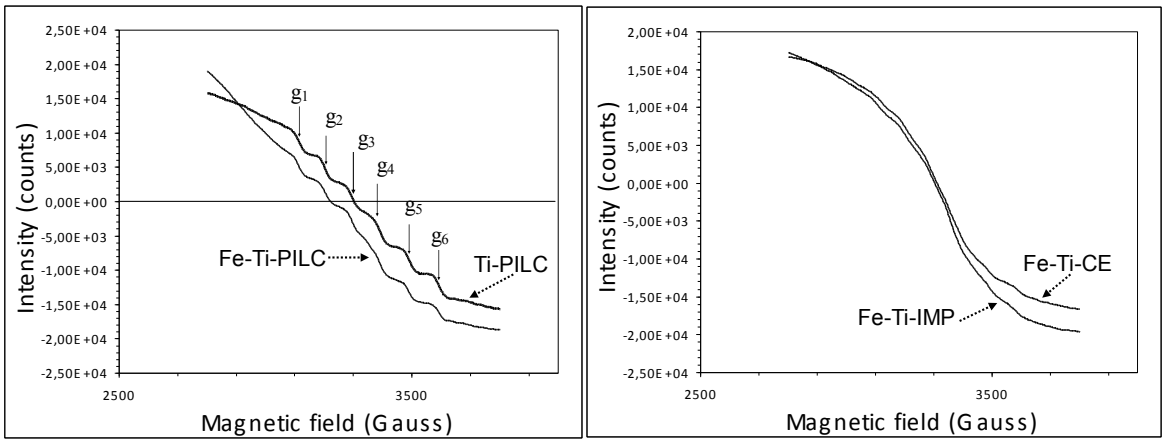

Fig. 5. Additional g-values to the central line in the EPR spectra of the Ti-PILC and Fe-Ti-PILC.

Shelef, 2000; Hernández *et al*., 2006; Menezes *et al*., 2006; Umamaheswari *et al*., 2006), but in clay minerals it is attributed to the presence of iron in the octahedral layers. The broad signal around g=2.034 is attributed to the formation of Fe^{3+} species (electron spin S = 5/2) in clusters (oxide nanoparticles), where the iron ions have an octahedral symmetry and the interactions among spin magnetic moments are enormously favored into the population of electrons (Kucherov and Shelef, 2000; Hernández *et al*., 2006; Menezes *et al*., 2006; Umamaheswari *et al*., 2006).

The intensity of EPR signals of the Ti-PILC solid is very similar to that for bentonite (Figure 3a), but the intensity around g=2.034 for the Fe-Ti-PILC solid is higher than those (Figure 3b). Also, on the EPR spectra of the Fe-Ti-IMP and Fe-Ti-CE samples a small increase of intensity was observed (Figures 3c and 3d). This variation in the EPR intensities is due to the incorporation of iron cations in the solids, being Fe-Ti-PILC the material with higher incorporation of iron. On the other hand, a particular spectroscopic behavior of the Fe-Ti-PILC sample is observed, since

the central g-value was shifted to low magnetic field at g=2.091 (Figure 4). This change in the central line position of the EPR spectrum is a result of the structural incorporation of the Fe^{3+} ions in the TiO_2 lattice (isomorphic substitution, as suggested in previous work (Carriazo *et al*., 2010)). Figure 4 shows exactly the same central g-value for all the other studied materials, but slightly different for Fe-Ti-PILC, which is in agreement with the fact that an incorporation of Fe^{3+} ions into the TiO_2 structure was not expected by using those synthesis procedures corresponding to the Ti-PILC, Fe-Ti-IMP or Fe-Ti-CE solids. Furthermore, as shown in Figures 4 and 5 additional g-values were observed for the Ti-PILC and Fe-Ti-PILC samples, which are directly associated to the TiO_2 incorporation.

Titanium dioxide (TiO_2) contains Ti^{4+} in its structure, which does not have unpaired electrons in its electronic configuration and so no EPR-signal should be observed, but some paramagnetic centers may be arisen from electron trapping sites due to electrons or oxygen radicals in oxygen vacancies (e^-/hole/Ti^{4+}, $O^{\bullet-}/Ti^{4+}$ or $O_2^{\bullet-}/Ti^{4+}$ species) with different coordination and environments (Coronado *et al*., 2002; Wang *et al*., 2011). The additional g-values (g_1 to g_6) around the central line (Figure 5 and Table 1) are a consequence of both the structural oxygen vacancies with trapped electrons (e^-/hole/Ti^{4+}) and the other electron trapping sites ($O^{\bullet-}//Ti^{4+}$ or $O_2^{\bullet-}//Ti^{4+}$) (Coronado *et al*., 2002; Hurum *et al*., 2006; Carter *et al*., 2007; Scotti *et al*., 2009; Wang *et al*., 2011), all of these sites originated through the synthesis of solids. These six lines (g_1 to g_6) in Ti-PILC and Fe-Ti-PILC can be explained from the hyperfine interactions between trapped electron species (electron trapping sites) and the titanium nuclei. Therefore the Ti^{4+} ions can be considered as Ti^{3+} because of the partial reduction of Ti^{4+} ($e^- + Ti^{4+} = Ti^{3+}$), and so Ti^{3+} ions have an electronic configuration with an unpaired electron ($Ar3d^1$), showing hyperfine interaction between this electron and the nucleus of titanium (^{47}Ti with nuclear spin $I = 5/2$) to give a sextet in the EPR spectrum and an experimental hyperfine splitting constant of 91.733 gauss in both cases for Ti-PILC and Fe-Ti-PILC (Bielski *et al*., 1967). In EPR, the number of lines originated from hyperfine interactions is determined by $2I + 1$, which can explain the six symmetrical lines observed.

These additional g-values are absent in the Fe-Ti-IMP and Fe-Ti-CE probably due to the further procedures carried out in the synthesis of these solids, such as impregnation and cationic exchange followed by a second calcination at 400 °C in each case. On the other hand, oxygen vacancies with trapped electron are very important for the photo-catalytic behavior of both Ti-PILC and Fe-Ti-PILC solids (the more active solids in previous work (Carriazo *et al*., 2010)), because of such cavities have acceptor energy levels closer to the electron conduction band (Liu *et al*., 2005). That phenomenon leads to a slight decrease of the band-gap in solid structures allowing absorption of radiation with smaller energy (light closer to the visible region than pure UV radiation).

Conclusions

TiO_2 and Fe/TiO_2 delaminated clays was characterized by electron paramagnetic resonance (EPR), which showed the characteristic g-values of iron ions (Fe^{3+}) in different structural environment of clay: octahedral-layer sites and oxide nanoclusters.

Table 1. g-values of additional lines observed in EPR spectra of Ti-PILC and Fe-Ti-PILC solids.

Ti-PILC		Fe-Ti-PILC	
Magnetic field (Gauss)	g	Magnetic field (Gauss)	g
3120	$g_1 = 2.162$	3119	$g_1 = 2.162$
3207	$g_2 = 2.103$	3209	$g_2 = 2.102$
3315	$g_3 = 2.034$	3225	$g_3 = 2.091$
3383	$g_4 = 1.994$	3384	$g_4 = 1.993$
3492	$g_5 = 1.931$	3490	$g_5 = 1.932$
3595	$g_6 = 1.876$	3592	$g_6 = 1.877$

Additionally, a significant shift of the central g-value as a consequence of Fe^{3+} substitution in the TiO_2 structure was observed for the solid obtained by direct addition of iron ions in the titanium aqueous solution (solid named Fe-Ti-PILC). A series of additional g-values symmetrically distributed around the central absorption line was observed for the TiO_2 nanoparticles included in the clay mineral, which were attributed to both structural oxygen vacancies (holes) with trapped electrons and other electron trapping sites remained in the TiO_2 framework after synthesis.

Acknowledgments

The authors gratefully would like to acknowledge the Universidad Nacional de Colombia (Facultad de Ciencias, Sede Bogotá) for facilitating this investigation. A part of this work was developed at the Lab 125 (Lab-DRES: Laboratorio de Diseño y Reactividad de Estructuras Sólidas) of the UNAL-Bogotá.

References

Ambrus Z., Balázs N., Alapi T., Wittmann G., Sipos P., Dombi A. and Mogyorósi K. (2008). Synthesis, structure and photocatalytic properties of Fe(III)-doped TiO_2 prepared from $TiCl_3$. *Applied Catalysis B 81*, 27-37.

Bhargava S. K., Tardio J., Prasad J., Foger K., Akolekar D. B. and Gocott S. C. (2006). Wet oxidation and catalytic wet oxidation. *Industrial and Engineering Chemistry Research 45*, 1221-1258.

Bielski B. H. J. and Gebicki J. M. (1967). *Atlas of Electron Spin Resonance Spectra*, first ed. Academic Press, New York.

Carriazo J. G., Guélou E., Barrault J., Tatibouët J. M., Molina R. and Moreno S. (2005). Catalytic wet peroxide oxidation of phenol by pillared clays containing Al-Ce-Fe. *Water Research 39*, 3891-3899.

Carriazo J. G., Molina R. and Moreno S. (2008). A study on Al and Al-Ce-Fe pillaring species and their catalytic potential as they are supported on a bentonite. *Applied Catalysis A 334*, 168-172.

Carriazo J. G, Molina R. and Moreno S. (2007). Caracterización estructural y textural de una bentonita colombiana. *Revista Colombiana de Química 36*, 213-225.

Carriazo J. G., Moreno-Forero M., Molina R. A and Moreno S. (2010). Incorporation of titanium and titanium-iron species inside a smectite-type mineral for photocatalysis. *Applied Clay Science 50*, 401-408.

Carter E., Carley A. F., and Murphy D. M. (2007). Evidence for O_2- Radical stabilization at surface oxygen vacancies on polycrystalline TiO_2. *Journal of Physical Chemistry C 111*, 10630-10638.

Chong S. V., Xia J., Suresh N., Yamaki K. and Kadowaki K. (2008). Tailoring the magnetization behavior of Co-doped titanium dioxide nanobelts. *Solid State Communication 148*, 345-349.

Cordischi D., Gazzoli D., Occhiuzzi M. and Valigi, M. (2000). Redox Behavior of VI B transition metal ions in rutile TiO_2 solid solutions: an XRD and EPR study. *Journal of Solid State Chemistry 152*, 412-420.

Coronado J. M., Maira A. J., Martínez-Arias A., Conesa J. C. and Soria J. (2002). EPR study of the radicals formed upon UV irradiation of ceria-based photocatalysts. *Journal of Photochemistry and Photobiology A 150*, 213-221.

Crittenden J. C., Liu J., Hand D. W. and Perram D. L. (1997). Photocatalytic oxidation of chlorinated hydrocarbons in water. *Water Research 31*, 429-438.

Di Paola A., García-López E., Ikeda S., Marci G., Ohtani B. and Palmisano L. (2002). Photocatalytic degradation of organic compounds in aqueous systems by transition metal doped polycrystalline TiO_2. *Catalysis Today 75*, 87-93.

Güler S., Rameev B., Khaibullin R., Lopatin O. and Aktas B. (2009). EPR study of Mn-implanted single crystal TiO_2. *Journal of Physics: Conference Series 153*, 1-6.

Hernández Y., Carriazo J. G., and Almanza O. A. (2006). Characterization by XRD and electron paramagnetic resonance (EPR) of waste materials from "Cerro Matoso" Mine

(Colombia). *Materials Characterization 57*, 44-49.

Hurum D. C., Agrios A. G., Crist S. E., Gray K. A., Rajh T. and Thurnauer M. C. (2006). Probing reaction mechanisms in mixed phase TiO_2 by EPR. *Journal of Electron Spectroscopy and Related Phenomena 150*, 155-163.

Iurascu B., Siminiceanu I., Vione D., Vicente M. A. and Gil A. (2009). Phenol degradation in water through a heterogeneous photo-Fenton process catalyzed by Fe-treated laponite. *Water Research 43*, 1313-1322.

Janes R., Knightley L. J. and Harding C. J. (2004). Structural and spectroscopic studies of iron (III) doped titania powders prepared by sol-gel synthesis and hydrothermal processing. *Dyes and Pigments 62*, 199-202.

Kucherov A. and Shelef M. (2000). Quantitative determination of isolated Fe^{3+} cations in FeHZSM-5 catalysts by ESR. *Journal of Catalysis 195*, 106-112.

Liotta L. F., Gruttadauria M., Di Carlo G., Perrini G. and Librando V. (2009). Heterogeneous catalytic degradation of phenolic substrates: catalysis activity. *Journal of Hazardous Materials 162*, 588-606.

Liu S. and Chen Y. (2009). Enhanced photocatalytic activity of TiO_2 powders doped by Fe unevenly. *Catalysis Communication 10*, 894-899.

Liu Z. L., Cui Z. L. and Zhang Z. K. (2005). The structural defects and UV-VIS spectral characterization of TiO_2 particles doped in the lattice with Cr^{3+} cations. *Materials Characterization 54*, 123-129.

Menezes W., Camargo P., Oliveira M., Evans D., Soares J. and Zarbin A. (2006). Sol-gel processing of a bimetallic alkoxide precursor confined in porous glass matrix: A route to novel glass/metal oxide nanocomposites. *Journal of Colloid and Interface Sciences 299*, 291-296.

Pal B., Sharon M. and Nogami G. (1999). Preparation and characterization of TiO_2/Fe_2O_3 binary mixed and its photocatalytic properties. *Materials Chemistry and Physics 59*, 254-261.

Perathoner S. and Centi G. (2005). Wet hydrogen peroxide catalytic oxidation (WHPCO) of organic waste in agro-food and industrial streams. *Topics in Catalysis 33*, 207-224.

Re R., Pellegrini N., Proteggente A., Pannala A., Yang M. and Rice-Evans C. (1999). Antioxidant activity applying an improved ABTS radical cation decolorization assay. *Free Radical Biology and Medicine 26*, 1231-1237.

Scott S. L., Chen W. J., Bakac A. and Espenson J. H. (1993). Spectroscopic parameters, electrode potentials, acid ionization constants, and electron exchange rates of the 2,2'-Azinobis (3-ethylbenzothiazolineine-6-sulfonate) radicals and ions. *Journal of Physical Chemistry 97*, 6710-6714.

Scotti R., D'Arienzo M., Testino A. and Morazzoni F., (2009). Photocatalytic mineralization of phenol catalyzed by pure and mixed phase hydrothermal titanium dioxide. *Applied Catalysis B 88*, 497-504.

Soria J., Sanz J., Sobrados I., Coronado J. M., Fresno F. and Hernández-Alonso M. D. (2007). Magnetic resonance study of the defects influence on the surface characteristics of nanosize anatase. *Catalysis Today 129*, 240-246.

Umamaheswari V., Bohlmann W., Poppl A., Vinu A. and Hartmann M. (2006). Spectroscopic characterization of iron-containing MCM-58. *Microporous and Mesoporous Materials 89*, 47-57.

Wang Z., Ma W., Chen C., Ji H. and Zhao J. (2011). Probing paramagnetic species in titania-based heterogeneous photocatalysis by electron spin resonance (ESR) spectroscopy-A minireview. *Chemical Engineering Journal 170*, 353-362.

Yang S., Zhu W., Wang J. and Chen Z. (2008). Catalytic wet air oxidation of phenol over CeO_2-TiO_2 catalyst in the batch reactor and the packed-bed reactor. *Journal of Hazardous Materials 153*, 1248-1253.

Ye F., Tsumura T., Nakata K. and Ohmori A. (2008). Dependence of photocatalytic activity on the compositions and photo-absorption of functional TiO_2-Fe_3O_4 coatings deposited by plasma spray. *Materials Science and Engineering B 148*, 154-161.

Zalibera M., Stasko A., Slebodová A., Jancovicová V., Cermákoá T. and Brezová, V. (2008). Antioxidant and radical-scavenging activities of Slovak honeys- An electron paramagnetic resonance study. *Food Chemistry 110*, 512-521.

Zhu J., Chen F., Zhang J., Chen H. and Anpo M. (2006). Fe^{3+}-TiO_2 photocatalysts prepared by combining sol-gel method with hydrothermal treatment and their characterization. *Journal of Photochemistry and Photobiology A 180*, 196-204.

Zhu J., Zheng W., He B., Zhang J. and Anpo M. (2004). Characterization of Fe-TiO_2 photocatalysts synthesized by hydrothermal method and their photocatalytic reactivity for photodegradation of XRG dye diluted in water. *Journal of Molecular Catalysis A 216*, 35-43.